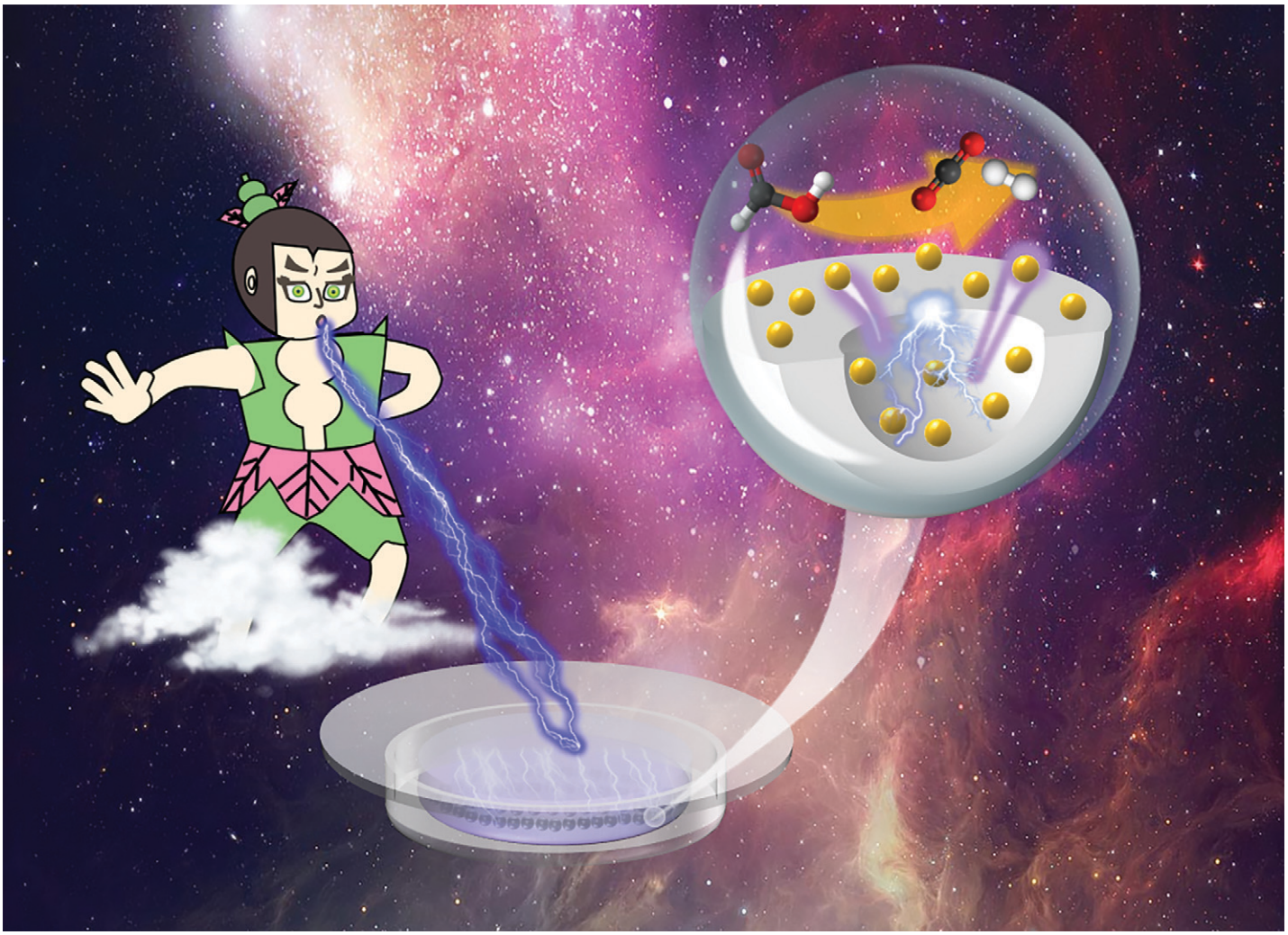

Showcasing research from Prof. Lanbo Di and Prof. Xiuling Zhang's group at Dalian University, China and Prof. Xin Tu's group at University of Liverpool, UK.

Dehydrogenation of formic acid over Pd/C catalysts: insight into the cold plasma treatment

A promising and emerging cold plasma process has been developed and explored for the fast synthesis of highly active Pd/C catalysts with enhanced performance for formic acid dehydrogenation. This work has great potential to open a green and sustainable route for fast and controllable synthesis of a range of highly active and stable supported metal catalysts.

As featured in:

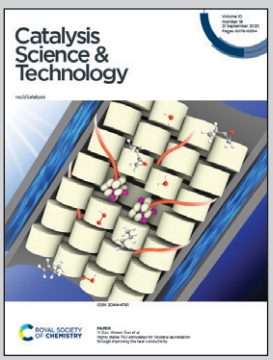

See Lanbo Di, Xiuling Zhang, Xin Tu *et al.*, *Catal. Sci. Technol.*, 2020, **10**, 6151.

ROYAL SOCIETY OF CHEMISTRY

rsc.li/catalysis

Registered charity number: 207890

Catalysis Science & Technology

ROYAL SOCIETY OF CHEMISTRY

PAPER

View Article Online
View Journal | View Issue

Cite this: *Catal. Sci. Technol.*, 2020, **10**, 6151

Dehydrogenation of formic acid over Pd/C catalysts: insight into the cold plasma treatment

Lanbo Di, *[a] Jingsen Zhang,[a] Michael Craven,[b] Yaolin Wang,[b] Hongyang Wang,[a] Xiuling Zhang*[a] and Xin Tu *[b]

Safe and efficient generation of renewable hydrogen *via* dehydrogenation of cheap and sustainable formic acid using supported Pd catalysts has attracted significant interest. Non-thermal (cold) plasma is demonstrably a fast and environmentally friendly method for synthesizing high-performance supported metal catalysts; however, the synthesis mechanism in the plasma treatment of catalysts still remains obscure. In this work, we investigate formic acid dehydrogenation over activated carbon supported Pd catalysts synthesized using four different methods: thermal treatment (Pd/C-C), plasma treatment (Pd/C-P), thermal treatment followed by plasma treatment (Pd/C-CP), and plasma treatment followed by thermal treatment (Pd/C-PC). The influence of different catalyst treatment methods on the characteristics and dehydrogenation performance of the Pd/C catalysts has been evaluated and discussed. The activity of the Pd/C catalysts for formic acid dehydrogenation follows the order: Pd/C-CP > Pd/C-C > Pd/C-P > Pd/C-PC. The turnover frequency ($TOF_{initial}$) over Pd/C-CP is 1.4, 2.9, and 1.4 times higher than that over Pd/C-C, Pd/C-P and Pd/C-PC, respectively. The activation energy for Pd/C-CP (34.6 kJ mol^{-1}) is much lower than that reported for monometallic Pd catalysts. The excellent performance of the Pd/C-CP catalyst can be attributed to the small size and high dispersion of Pd nanoparticles, the high concentration of metallic Pd, and the high Pd/C atomic ratio resulting from the migration of the electroneutral Pd species under the Coulomb repulsion effect of the electrons in the plasma. The high performance of the Pd/C-C catalyst was attributed to the small and highly dispersed Pd nanoparticles formed due to the strong interaction between the activated carbon support and $PdCl_4^{2-}$ ions. The Pd/C-P catalyst exhibits poor performance on account of the low reduction rate of $PdCl_4^{2-}$ ions. The poorest performance, from Pd/C-PC, was ascribed to the large size of the Pd nanoparticles that were formed due to the disturbance of the interaction between the activated carbon support and the $PdCl_4^{2-}$ ions during the preparation of the Pd/C-P catalyst. In conclusion, thermal treatment of Pd/C – prepared using a simple incipient wetness procedure – followed by plasma treatment is an effective method for the synthesis of a high-performance Pd/C catalyst.

Received 12th January 2020,
Accepted 21st June 2020

DOI: 10.1039/d0cy00055h

rsc.li/catalysis

1. Introduction

The International Energy Agency reported that global emissions of carbon dioxide reached a record high of 33bn tonnes in 2018 (up 1.7% from the previous year) as the energy demand rose by 2.3%.[1] The growth in energy demand was met mainly by the use of fossil fuels, hence the rise in carbon dioxide (CO_2) emissions. The development of sustainable and renewable energy that does not rely on fossil fuels is, therefore, a key environmental and energy challenge to reduce carbon footprint and to achieve a low-carbon circular economy.

Hydrogen is a promising green energy carrier that can be produced from renewable and sustainable resources.[2] It can be used in fuel cells to generate electricity, or power and heat, and forms only water as a by-product. It is often stored using pressurized or cryogenic liquefaction methods, which are both expensive and require extreme conditions to achieve. There is, therefore, an urgent requirement to develop cheaper and safer techniques to store and generate hydrogen under mild conditions for common use. Adopting renewable and sustainable chemicals as hydrogen carriers is an ideal method to solve this problem.[3,4]

Formic acid (HCOOH) is considered an ideal hydrogen carrier due to its ease of storage and transportation. It is also nontoxic, cheap, and renewable, and has a high hydrogen storage capacity (53 g H_2 per l).[5] Hydrogen can be released from formic acid *via* two reaction pathways:[6–11]

Dehydrogenation

[a] *College of Physical Science and Technology, Dalian University, Dalian 116622, China. E-mail: dilanbo@163.com, xiulz@sina.com*
[b] *Department of Electrical Engineering and Electronics, University of Liverpool, Liverpool L69 3GJ, UK. E-mail: xin.tu@liverpool.ac.uk*

$$HCOOH(l) \rightleftharpoons H_2(g) + CO_2(g),\ \Delta G_{298\ K} = -35.0\ kJ\ mol^{-1}$$

Dehydration

$$HCOOH(l) \rightleftharpoons H_2O(l) + CO(g),\ \Delta G_{298\ K} = -14.9\ kJ\ mol^{-1}$$

Dehydrogenation is the desirable reaction as hydrogen is released – along with CO_2 – whereas the dehydration reaction produces water and carbon monoxide (CO), and thus reduces the hydrogen production efficiency.[12–14] The use of a suitable catalyst can favour the release of hydrogen through the dehydrogenation reaction while suppressing the dehydration reaction, which is important as CO can poison the catalyst.

Recently, the use of supported Pd catalysts in the efficient generation of hydrogen from formic acid has attracted significant interest due to their high performance under mild conditions.[15–17] However, in the preparation of supported Pd catalysts (*e.g.*, Pd/activated carbon), these catalysts are often reduced by chemical reduction using toxic or excess reducing agents, such as sodium borohydride, citric acid and ethanol. The use of such a wet method is time-consuming and not environmentally friendly. Supported Pd catalysts can also be reduced by thermal reduction for a few hours at high temperatures, which has the potential to cause the aggregation of Pd particles on the catalyst surfaces. Cold plasma offers an alternative dry method for the green, fast and low temperature reduction of supported Pd catalysts with enhanced catalyst activity and stability.

In non-equilibrium cold plasmas, the gas kinetic temperature remains low (near room temperature), while the electrons produced are highly energetic and collide with the background gas, creating a cascade of reactive species including free radicals, excited-state and ground-state molecules, ions, and atoms.[18] In addition, plasma induced reactions are fast and plasma processes can be switched on and off instantly. These advantages make cold plasmas attractive for the rapid preparation of highly active and selective catalysts at low temperatures, including supported metal catalysts.[19–21] Indeed, the Coulomb repulsion effect of the electrons – resulting from the strong electric field of the plasma – generally favors the preparation of small and highly dispersed metal nanoparticles (NPs) on the catalyst support, and enhances the metal–support interactions.[19–24] The fast (generally <1 h) and low temperature plasma treatment is also beneficial for the synthesis of small and amorphous metal nanoparticles.[25,26] The degree of alloying of multi-metal nanoparticles can also be tuned using cold plasma treatment instead of using conventional high-temperature thermal calcination processes with longer treatment times.[21,27,28] In addition, cold plasmas are very promising for preparing metal nanoparticles supported on thermally sensitive materials[29,30] due to their low-temperatures and fast processes, and they can even be used to selectively synthesize preferred crystal faces.[30,31]

Cold plasma can also be used to reduce supported metal catalysts. The energetic electrons generated in cold plasma can directly reduce metal ions at low pressures,[20] while active hydrogen species or excited molecules (*e.g.*, excited-state CO molecules[32]) generally serve as reducing agents in atmospheric pressure cold plasmas as they are present in larger concentrations at higher pressures due to more frequent collisions between the energetic electrons and the gas molecules.[19,33] Increasing efforts have been devoted to investigating the use of cold plasmas for the treatment of supported metal catalysts. Liu and co-workers have conducted pioneering work in plasma preparation of catalysts and the recent advances in this emerging research topic have been summarized in their review paper.[20] Chu *et al.* used a glow discharge to prepare supported cobalt catalysts for Fischer–Tropsch synthesis.[34,35] They found that the plasma treatment diminished the reducibility of the Co catalysts. Similar findings have been reported by other groups.[36–38] In addition, Chu *et al.* found that increasing the specific input energy of the glow discharge reduced the size of cobalt nanoparticles.[39] Similarly, Di *et al.* used an atmospheric pressure cold plasma for the synthesis of Ag/TiO_2 catalysts and found that increasing the discharge voltage led to a blue shift and narrowed surface plasmon resonance absorption in the UV-vis spectra of the catalysts.[40] However, cold plasma synthesis and treatment of catalysts is a complex process due to the simultaneous physical and chemical interactions between the plasma and catalysts. The synthesis mechanism in the plasma treatment of catalysts is still not clear and the contribution of cold plasma to the reduced metal particle size and the enhanced metal dispersion on the catalyst surfaces has not yet been fully explored and understood. Therefore, significant fundamental research is essential to gain new insights into the role of cold plasmas in the synthesis and treatment of highly active supported metal catalysts.

In this work, we report formic acid dehydrogenation for hydrogen production over activated carbon (AC) supported Pd catalysts synthesized using different methods: thermal treatment (Pd/C-C), plasma treatment (Pd/C-P), thermal treatment followed by plasma treatment (Pd/C-CP), and plasma treatment followed by thermal treatment (Pd/C-PC). The effect of thermal treatment, plasma treatment and their combinations on the characteristics and dehydrogenation performance of the Pd/C catalysts has been investigated through comprehensive catalyst characterization to elucidate the role of cold plasma in the treatment of the catalysts. The Pd/C-CP catalyst exhibits the highest activity for formic acid dehydrogenation due to the formation of smaller and highly dispersed Pd nanoparticles, its high concentration of metallic Pd, and its high Pd/C atomic ratio resulting from the migration of the electroneutral Pd species under the Coulomb repulsion effect of electrons in the plasma.

2. Experimental

2.1 Plasma reactor

A plate-to-plate dielectric barrier discharge (DBD) reactor was used for catalyst treatment in this work. The DBD reactor was

composed of a quartz tube and two stainless-steel electrodes (Φ50 mm) with a discharge gap of 4 mm. The reactor was powered by a high-voltage power supply (CTP-2000K, Nanjing Suman) with a sinusoidal peak voltage of up to 36.0 kV and a frequency of 13.6 kHz. Further details of the DBD reactor can be found in our previous work.[24] High purity hydrogen (>99.999%) was used as a working gas with a fixed flow rate of 100 ml min^{-1}. The catalysts were uniformly placed in the DBD reactor to ensure uniform plasma treatment. Each catalyst sample was treated three times, and each treatment lasted 2 min.

2.2 Catalyst preparation

Activated carbon (Beijing Guanghua Timber Mill) with a size of 40–60 mesh was firstly pre-oxidized with 30% HNO_3 at 85 °C for 5 h, and then washed with deionized water until the solution reached a pH of 7.[41] The pre-oxidized activated carbon was then dried at 120 °C for 2 h.

The activated carbon supported Pd catalyst was prepared using the incipient wetness impregnation method with $PdCl_2$ (AR, Tianjin Kemiou) as a metal precursor. The as-synthesized Pd/C catalyst was denoted Pd/C-As. The nominal Pd loading of the Pd/C catalysts was 5.0 wt%. To understand the effect of plasma treatment on Pd/C catalysts for formic acid dehydrogenation, various Pd/C catalysts were prepared through the modification of the as-synthesized Pd/C catalyst using cold plasma and/or conventional thermal approaches.

A portion of Pd/C-As was treated using a hydrogen DBD at ambient pressure, and the obtained catalyst was denoted Pd/C-P. Another portion of Pd/C-As was treated thermally in a temperature-programmed tubular quartz reactor using high purity hydrogen (>99.999%) at 300 °C for 2 h, and the obtained catalyst was denoted Pd/C-C. The flow rate of hydrogen was fixed at 100 ml min^{-1} with a heating rate of 5 °C min^{-1}.

Additionally, 0.5 g of Pd/C-P obtained from the plasma treatment was further treated thermally using the same experimental conditions used to treat the Pd/C-C catalyst, and the obtained catalyst was labelled Pd/C-PC. A portion of the Pd/C-C catalyst (0.5 g) obtained by thermal treatment was further modified with the plasma using the same experimental parameters as those for synthesizing the Pd/C-P catalyst, and the obtained catalyst was denoted Pd/C-CP.

For quick reference, the Pd/C catalysts and the corresponding preparation methods are summarized and listed in Table 1.

Table 1 Different preparation methods of the Pd/C catalysts

Indexing	Preparation method
Pd/C-As	As-synthesized
Pd/C-C	Thermal treatment
Pd/C-P	Plasma treatment
Pd/C-CP	Thermal treatment followed by plasma treatment
Pd/C-PC	Plasma treatment followed by thermal treatment

2.3 Catalyst characterization

X-ray diffraction (XRD) patterns of the Pd/C catalysts were recorded using a DX-2700 (Dandong Haoyuan Instrument Co. Ltd., China) X-ray diffractometer with Cu Kα radiation (λ = 0.154178 nm) operating at 40 kV and 30 mA. Transmission electron microscopy (TEM) images of the catalysts were obtained by using an HT7700 transmission electron microscope (Hitachi, Japan) at an accelerating voltage of 120 kV. The size and size distribution of the Pd nanoparticles were obtained by measuring more than 100 Pd nanoparticles. To understand the surface composition and the oxidation states of the Pd species in the catalysts, X-ray photoelectron spectroscopy (XPS) analysis was carried out using an ESCALAB250 (Thermo Fisher Scientific, USA) X-ray photoelectron spectrometer system equipped with a monochromatic AlKα (1486.6 eV) X-ray source. All binding energies were calibrated to C1s at 284.6 eV. The atomic ratios of Pd/C for the Pd/C catalysts are obtained according to the XPS data (Table 2). The pore volume (V_p), pore size (D_p), and specific surface area (S_{BET}) of the catalysts were measured at 77 K using a NOVA2200e nitrogen gas adsorption/desorption analyzer (Quantachrome Corp., USA). Before each measurement, the samples were outgassed at 200 °C for 5 h. The adsorption and desorption data were obtained by the Barrett–Joyner–Halenda (BJH) model using the Halsey equation. Temperature-programmed reduction (TPR) of the catalysts was carried out using a Micromeritics (AutoChem II 2920) equipment. Before each TPR experiment, 180 mg catalyst was pretreated in Ar gas at 120 °C for 1 h, then cooled down to room temperature. The sample was then heated from room temperature to 600 °C at a ramping rate of 10 °C min^{-1} using a 10 vol% H_2/Ar gas mixture.

2.4 Activity tests

Formic acid dehydrogenation reactions were conducted in a two-necked 60 ml distillation flask with a magnetic stirrer (200 rpm stirring speed) to evaluate the catalytic activity of the different Pd/C catalysts. The flask was placed in a water bath at a pre-set temperature of 50 °C. In a typical run, the Pd/C catalyst (50 mg) and deionized water (10 ml) were first mixed in the flask. Once the temperature reached 50 °C, a mixture of 2 ml of 4 M formic acid (HCOOH, ≥96%, Sigma-Aldrich) and 8 ml of 4 M sodium formate (HCOONa, ≥96%, Sigma-Aldrich) was then injected into the flask using an injection syringe. The volume of the gas products generated

Table 2 The Pd composition and the atomic ratio of Pd/C in the Pd/C catalysts

	Pd composition (%)			
Sample	Pd^0	Pd^{II}	Pd^{IV}	Atomic ratio of Pd/C
Pd/C-C	37.4	33.5	29.1	0.004
Pd/C-P	35.4	35.9	28.7	0.011
Pd/C-CP	50.8	29.2	20.0	0.023
Pd/C-PC	40.6	28.8	30.6	0.006

was measured by recording the displacement of water in a measuring cylinder at 25 °C. The gas products were identified and evaluated using a gas chromatograph (Tianmei GC7890) equipped with a thermal conductivity detector (TCD). In this study, no CO was measured in the gas products.

The turnover frequency (TOF) was calculated according to the following equation:

$$\mathrm{TOF} = \frac{\text{moles of HCOOH converted into } H_2 \text{ and } CO_2}{\text{Dispersion}(\%) \times \text{moles of Pd} \;\; \text{metal loading} \times \text{reaction time}(\mathrm{h})}$$

where the metal dispersion was determined using the average particle size from the TEM analysis.

Results and discussion

Fig. 1 presents the XRD patterns of the Pd/C catalysts using various preparation methods, as well as the as-synthesized Pd/C-As. For all the Pd/C catalysts, two broad diffraction peaks centred at around 24.5° and 43.5° are assigned to the carbon structure of the activated carbon support. Compared to that of the as-synthesized Pd/C-As, the XRD pattern of Pd/C-PC exhibits obvious diffraction peaks at *ca.* 40.1° and 46.6°, consistent with the (111) and (200) planes of the face-centred cubic (fcc) structure of Pd (JCPDS, no. 46-1043). However, only a weak diffraction peak at *ca.* 40.1° is found for Pd/C-C, Pd/C-P, and Pd/C-CP, suggesting that Pd species can be highly dispersed on the surface of the activated carbon. The sizes of Pd nanoparticles (calculated using the Scherrer equation) in Pd/C-C, Pd/C-P, and Pd/C-CP are smaller than that in Pd/C-PC.

To understand the composition and valence states of the Pd species on the catalyst surfaces, XPS measurements of Pd3d, C1s, O1s and Cl2p in the Pd/C catalysts were conducted, and the spectra are shown in Fig. 2. The Pd3d spectra (Fig. 2a) can be deconvoluted into three peaks at 335.8, 336.4, and 337.7 eV, corresponding to Pd^0, Pd^{II}, and Pd^{IV}, respectively.[41] Table 2 summarizes the composition of the Pd species determined from the Pd3d spectra. The composition of metallic Pd in Pd/C-P was 35.4%, close to that in Pd/C-C (37.4%). Compared to these two catalysts, the combination of thermal reduction and plasma reduction for catalyst treatment enhanced the Pd^0 composition for both the Pd/C-CP and Pd/C-PC catalysts. However, the Pd^0 composition on the surface of Pd/C-PC (40.6%) was still ~25% lower than that of Pd/C-CP (50.8%), which could be attributed to the pre-treatment of the catalyst using the DBD plasma. Similar results were also observed by Chu and co-workers. They synthesized supported cobalt catalysts using a glow discharge cold plasma and found that the reducibility of Co was partially decreased for the plasma synthesized catalysts.[34,35,39]

The Pd/C atomic ratios of the different Pd/C catalysts are also listed in Table 2. The Pd/C-P catalyst with plasma treatment showed a much higher Pd/C atomic ratio than the Pd/C-C catalyst prepared by thermal treatment only. This may be explained by the effect of the plasma on the Pd precursor species, $PdCl_4^{2-}$: under the Coulomb repulsion effect of the plasma, the negatively charged $PdCl_4^{2-}$ ions and the Pd species formed in the Pd/C-P catalyst could migrate from the inner surface to the outer surface of the AC support, which enhanced the Pd/C atomic ratio. The thermal reduction of the Pd catalyst followed by plasma treatment was also found to enhance the Pd/C atomic ratio of the catalyst when compared with thermal treatment only. A similar phenomenon was also reported in previous studies using negative and neutral metal precursors.[25,36,40,42–45]

The AC that was pre-oxidized with nitric acid was positively charged and contained a large number of oxygen-containing groups (Fig. 2b and c), which can facilitate the interaction between the AC support and Pd precursor ($PdCl_4^{2-}$) in the Pd/C-As catalyst. For the Pd/C-CP catalyst, some of the Pd species were in the metallic state after thermal reduction, and had a weaker interaction with the AC compared to the AC and $PdCl_4^{2-}$ ions in the as-synthesized Pd/C-As. Therefore, more Pd species could migrate from the inner surface to the outer surface of the AC under the Coulomb repulsion effect in the plasma treatment. As a result, the Pd/C atomic ratio of Pd/C-CP (0.023) was significantly higher than that of Pd/C-C (0.004).

Plasma treatment of the Pd catalyst before thermal reduction (Pd/C-PC) resulted in a much lower Pd/C atomic ratio than that of the catalyst treated with plasma only (Pd/C-P). This could be ascribed to the incomplete reduction of the Pd precursor by using the cold plasma. In this case, the strong interaction between the AC support and $PdCl_4^{2-}$ species may facilitate the migration of the Pd species from the outer surface of the AC support to their initial positions. However, the electrostatic attraction effects apply to the negatively charged $PdCl_4^{2-}$ species rather than the neutral Pd or PdO_x species. Therefore, the Pd/C atomic ratio of the Pd/C-PC catalyst was lower than that of Pd/C-P, but higher than that of Pd/C-C.

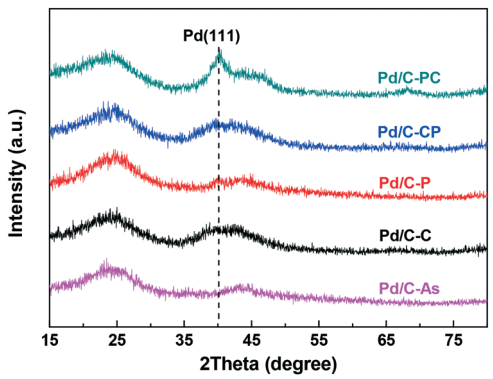

Fig. 1 XRD patterns of the Pd/C catalysts synthesized by various preparation methods, as well as the as-synthesized Pd/C-As.

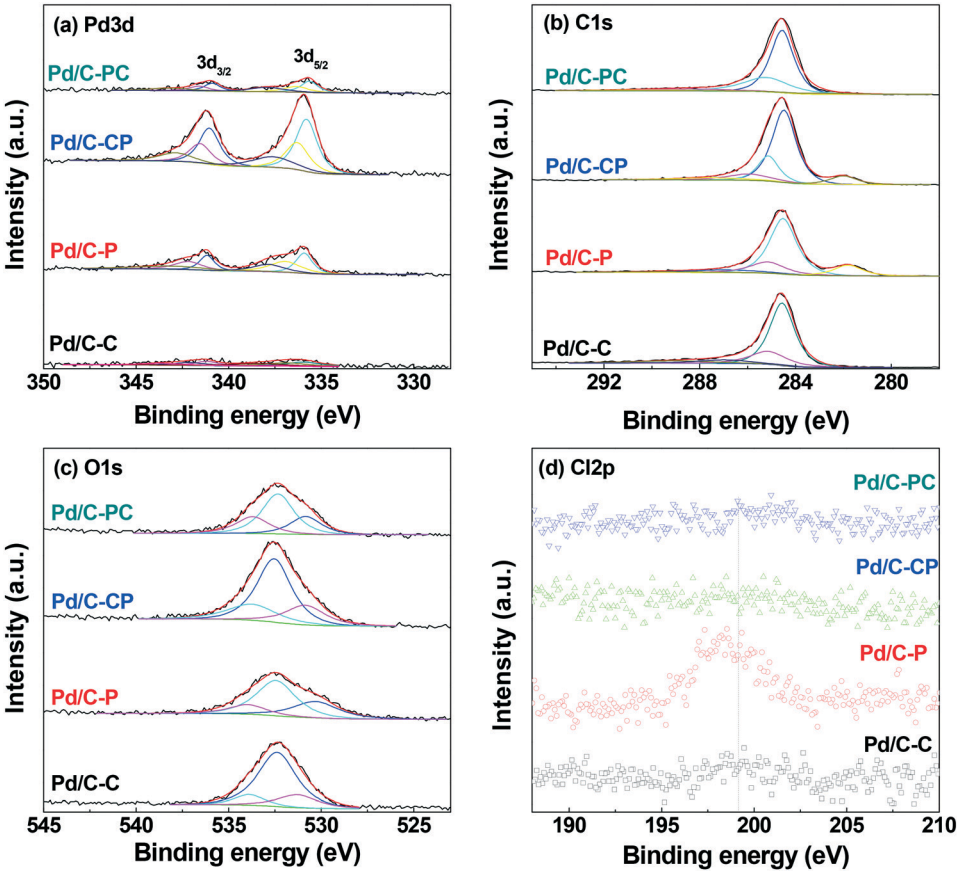

Fig. 2 XPS spectra of (a) Pd3d; (b) C1s; (c) O1s and (d) Cl2p in the Pd/C catalysts.

The C1s XPS spectra (Fig. 2b) of all the Pd/C catalysts were fitted with four peaks that are consistent with C–C (adventitious carbon contamination), C–OH, C═O, and COOH, respectively. Additionally, the O1s XPS spectra (Fig. 2c) of the Pd/C catalysts were deconvoluted into three peaks. These oxygen-containing functional groups anchor the Pd nanoparticles to the surface, helping to maintain their small size and high dispersion. One peak at 282.3 eV can also be deconvoluted from the C1s XPS spectra for Pd/C-P and Pd/C-CP, which was assigned to the negatively-charged carbon species directly bonded to Pd.[46,47] However, this peak (282.3 eV) cannot be detected in the XPS spectra of Pd/C-C and Pd/C-PC. The formation of negatively-charged carbon species can be ascribed to the cold plasma treatment with many high-mobility electrons, which can be removed by thermal treatment. Fig. 2d shows the Cl2p XPS spectra of the Pd/C catalysts. No peak corresponding to Cl species can be detected for Pd/C-C, Pd/C-CP, and Pd/C-PC, revealing that Cl species can be completely removed by thermal treatment and the combination of thermal treatment and plasma treatment. However, the Pd/C-P catalyst obtained by plasma treatment still retains some Cl species.

Fig. 3 and Table 3 show the influence of the preparation methods on the porous structure of the catalysts. At a relatively low pressure (p/p_0 = 0–0.2), the amount of adsorbed N_2 on the Pd/C samples increased rapidly, revealing the formation of a

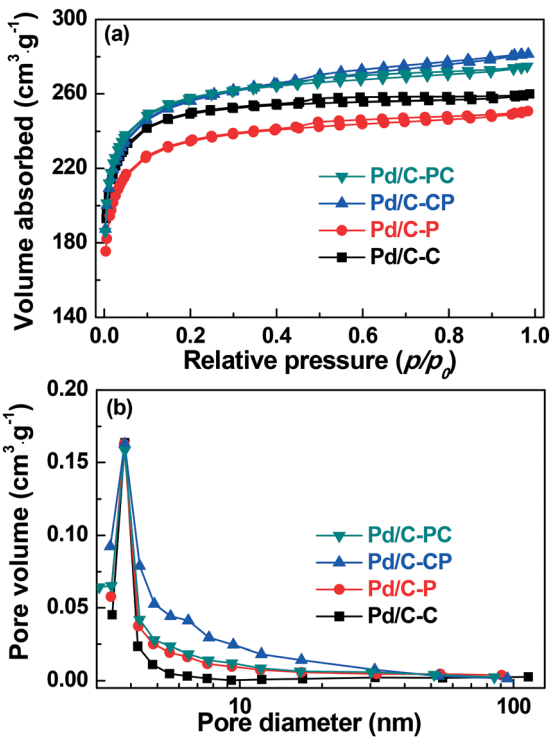

Fig. 3 (a) N_2 adsorption–desorption isotherms; (b) the corresponding pore size distributions of the Pd/C catalysts.

Table 3 The pore volumes (V_p), pore diameters (D_p), and specific surface areas (S_{BET}), as well as the size (D_{Pd}) and dispersion of the Pd nanoparticles, of the Pd/C catalysts

Sample	V_p ($cm^3\ g^{-1}$)	D_p (nm)	S_{BET} ($m^2\ g^{-1}$)	D_{Pd} (nm)	Dispersion (%)
Pd/C-C	0.014	3.81	762.6	2.5 ± 0.9	22.4
Pd/C-P	0.024	3.78	720.9	1.9 ± 0.6	29.5
Pd/C-CP	0.039	3.80	791.3	2.6 ± 1.0	21.5
Pd/C-PC	0.028	3.81	791.1	3.7 ± 1.2	15.1

type I isotherm which indicates a microporous structure. At a relative pressure of 0.4–0.99, a type IV isotherm with an H4 hysteresis loop was observed, suggesting the existence of a structure with slit-shaped mesopores. As shown in Fig. 3b, the pore size distribution of the Pd/C catalysts follows the order Pd/C-C < Pd/C-P ≈ Pd/C-PC < Pd/C-CP. This result is in line with the change of the Pd/C atomic ratio of these catalysts (Table 2), which can be attributed to the migration of the Pd species over the surface of the catalysts induced by the Coulomb repulsion effect of electrons.

Fig. 4 presents the TEM images of the different Pd/C catalysts and the corresponding size distribution of the Pd nanoparticles. The mean particle size of Pd (D_{Pd}) for Pd/C-C, Pd/C-P, Pd/C-CP, and Pd/C-PC is 2.5 ± 0.9, 1.9 ± 0.6, 2.6 ± 1.0, and 3.7 ± 1.2 nm, respectively (Table 3). Pd/C-C and Pd/C-CP have a similar mean Pd particle size, suggesting that plasma treatment had a limited effect on the size of the Pd nanoparticles. However, Pd/C-PC exhibits a larger Pd particle size compared to the other Pd/C catalysts, which can also be confirmed by the XRD results (Fig. 1).

As shown in Table 2, the Pd particle size in Pd/C-P was smaller than that in Pd/C-C, and the atomic ratio (Pd/C) of Pd/C-P (0.011) was much higher than that of Pd/C-C (0.004), which indicates that the distribution of the Pd species on the catalyst surfaces was significantly changed after the plasma treatment. In addition, the precursor ($PdCl_4^{2-}$) was not completely reduced in the preparation of the Pd/C-P catalyst, which can be further confirmed by the appearance of the residual Cl peak according to the Cl2p XPS spectra (Fig. 2d). In other words, the interaction of the activated carbon support with $PdCl_4^{2-}$ ions was destroyed by the DBD plasma, which facilitates the aggregation of the Pd nanoparticles with subsequent thermal treatment. Therefore, the Pd particle size of Pd/C-PC synthesized by cold plasma treatment followed by thermal treatment is much larger than that of the other Pd/C catalysts.

Fig. 5 shows the H_2-TPR profiles of the Pd/C catalysts. A negative peak at around 60 °C was observed for Pd/C-C, Pd/C-CP, and Pd/C-PC, while no negative peak was found in the TPR profile of Pd/C-P. The presence of this negative peak can be attributed to the desorption of H_2 gas from the metallic Pd surface at room temperature prior to the TPR process,[41,48] and its relative intensity is proportional to the Pd NP size. The absence of the negative peak for Pd/C-P can be ascribed to the formation of small Pd NPs (<2 nm)[49] and the low metallic Pd content (Table 2). Moreover, the relative intensity of this negative peak for Pd/C-C and Pd/C-CP was much weaker than that for Pd/C-PC, indicating that both Pd/C-C and Pd/C-CP

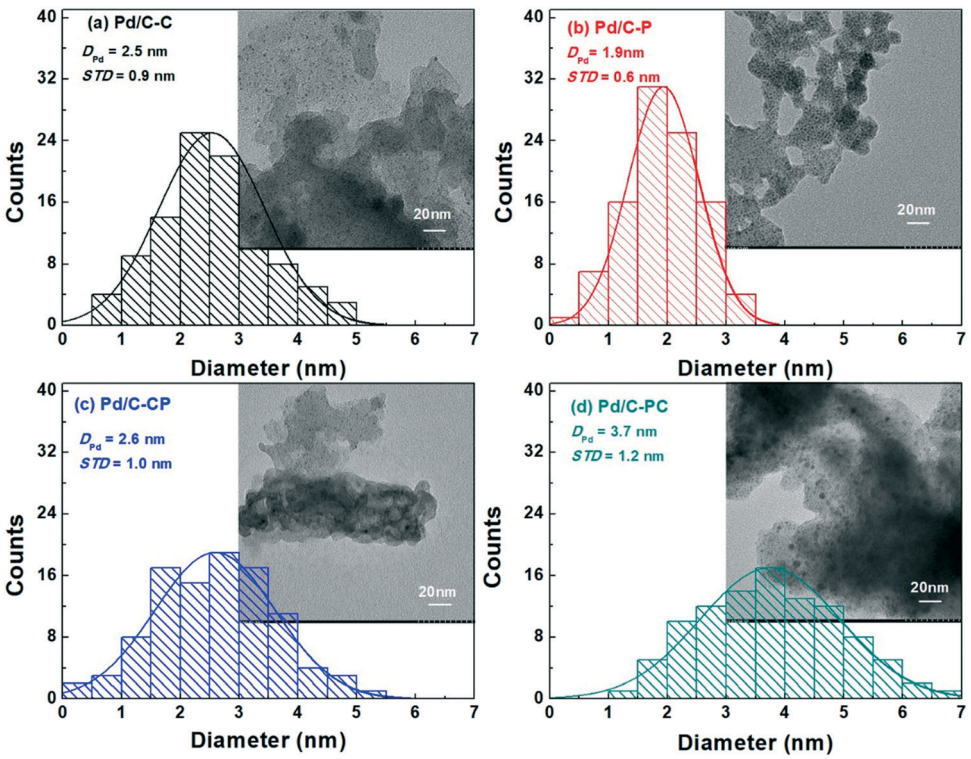

Fig. 4 Typical TEM images of the Pd/C catalysts and the corresponding histograms of the size distribution of the Pd nanoparticles (insets).

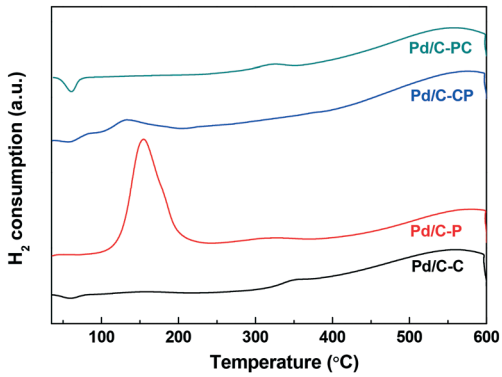

Fig. 5 TPR profiles of Pd/C-P, Pd/C-CP, Pd/C-PC and Pd/C-C.

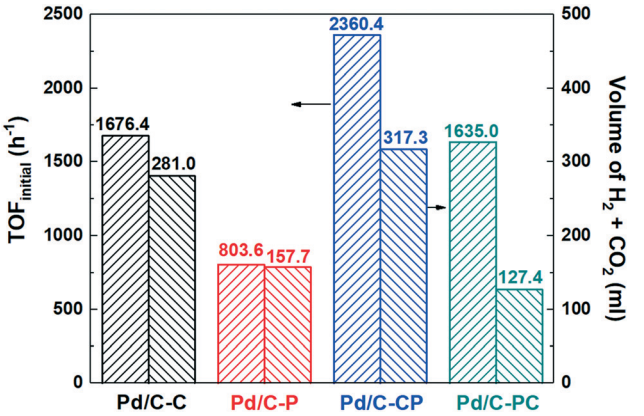

Fig. 7 The $TOF_{initial}$ and volume of generated CO_2 and H_2 of the Pd/C catalysts (reaction temperature 50 °C).

have Pd nanoparticles with smaller sizes. These are consistent with the variation of the Pd NP size observed by TEM.

The peaks at 100–400 °C are associated with the reduction of PdO_x species, while the peaks at higher and lower temperatures correspond to the reduction of subsurface PdO_x and surface PdO_x, respectively.[50] The TPR spectrum of Pd/C-P showed a dominant peak at around 154 °C, which can be ascribed to the formation of a high concentration of PdO_x and the high Pd/C atomic ratio. The positive peak at a lower temperature (*ca.* 132 °C) for Pd/C-CP can be assigned to the high concentration of surface PdO_x. These are consistent with the XPS results (Table 2).

Fig. 6 shows the total volume of CO_2 and H_2 produced *versus* time over the Pd/C catalysts. The volume of CO_2 and H_2 increased rapidly in the first 50 min of the reaction, then changed gradually until reaching a plateau at 200–250 min. The highest total volume (317.3 ml) of CO_2 and H_2 was achieved with a maximum formic acid conversion of 81.1% when using the Pd/C-CP catalyst. The activity of the Pd/C catalysts in the dehydrogenation of formic acid follows the order: Pd/C-CP > Pd/C-C > Pd/C-P > Pd/C-PC. Thermal treatment followed by plasma treatment could, therefore, be an effective method for the synthesis of high-performance Pd/C catalysts.

Fig. 7 shows the effect of the different Pd/C catalysts on the $TOF_{initial}$ and total volume of CO_2 and H_2. The total gas volume of CO_2 and H_2 over Pd/C-CP is 1.1, 2.0, and 2.5 times that over Pd/C-C, Pd/C-P and Pd/C-PC, respectively. The $TOF_{initial}$ over Pd/C-CP is 1.4, 2.9, and 1.4 times that over Pd/C-C, Pd/C-P and Pd/C-PC, respectively.

The influence of reaction temperature on formic acid dehydrogenation over the Pd/C-CP catalyst is shown in Fig. 8a. Increasing the reaction temperature from 20 to 50 °C significantly increased the total volume of CO_2 and H_2, while further increasing the temperature to 60 °C only provided a

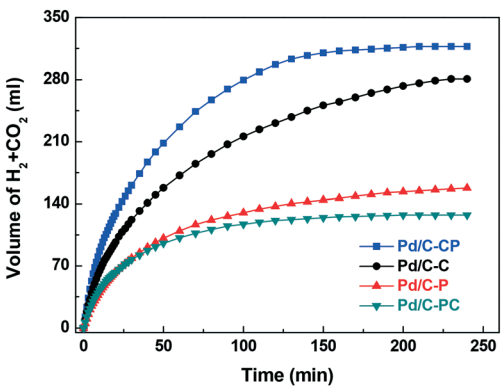

Fig. 6 The total volume of CO_2 and H_2 *versus* time over the Pd/C catalysts (reaction temperature 50 °C).

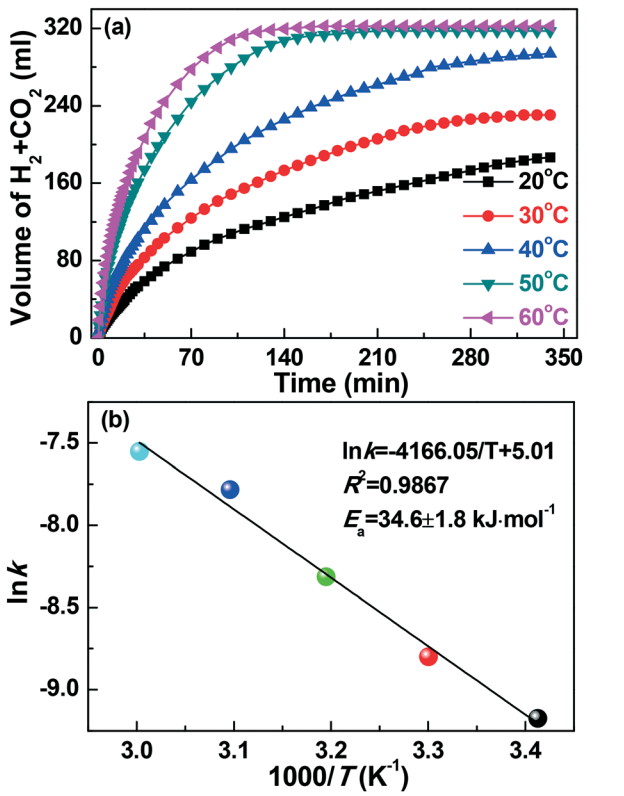

Fig. 8 (a) The total volume of CO_2 and H_2 *versus* time over the Pd/C-CP catalyst at different reaction temperatures; (b) the corresponding Arrhenius plot obtained according to the data taken from (a).

Table 4 Comparison of different Pd/C catalysts for formic acid dehydrogenation

Catalyst	T (°C)	Reagents	$TOF_{initial}$ (h^{-1})	E_a (kJ mol^{-1})	Ref.
Pd/C-CP	50	0.4 M FA & 1.6 M SF	2360.4	34.6 ± 1.8	This work
Pd/C	30	1.33 M FA	48.0	53.7	51
Pd/C	30	0.5 M FA	1136.0	39.0	52
Pd/C	50	6.0 M FA & 6.0 M SF	4452.0	39.6	53

FA: formic acid; SF: sodium formate.

slight improvement in the production of CO_2 and H_2. Fig. 8b shows a linear Arrhenius plot (R^2 = 0.9867) based on the results from Fig. 8a. An activation energy (E_a) of 34.6 ± 1.8 kJ mol^{-1} for the Pd/C-CP catalyst was determined from the slope of the Arrhenius plot. Table 4 compares the performance ($TOF_{initial}$ and E_a) of this catalyst (Pd/C-CP) in formic acid dehydrogenation with those reported in previous studies. The activation energy (E_a) of Pd/C-CP tested in this work is much lower than that reported for monometallic Pd catalysts in the literature.

Catalyst reuse experiments were conducted for the dehydrogenation of formic acid over Pd/C-CP to evaluate the stability of the catalyst, as shown in Fig. 9. The total volume of H_2 and CO_2 dropped slightly to 285 ml after the first reuse, but then there was very little loss in gas production between the second and fourth reuse cycles. This shows that the reused Pd/C-CP catalyst still exhibits remarkable catalytic activity without a significant loss in activity between subsequent cycles.

Fig. 10 presents the proposed mechanism for the formation of Pd NPs with different sizes and distributions in the Pd/C catalysts synthesized by different methods. As confirmed by the XRD (Fig. 1) and TEM (Fig. 4) results, Pd NPs that were small in size and highly dispersed were obtained for the Pd/C-C catalyst synthesized by thermal treatment due to the strong interaction between the positively-charged AC support and $PdCl_4^{2-}$ ions. Therefore, the Pd/C-C catalyst exhibited high activity for formic acid dehydrogenation.

For the Pd/C-CP catalyst prepared by thermal treatment followed by plasma treatment, the electroneutral Pd species are more prone to migrating from the inner surface to the outer surface of the AC support, resulting in a higher Pd/C atomic ratio. The smaller size and higher dispersion of the Pd NPs are maintained due to the Coulomb repulsion effect in the plasma. Additionally, the concentration of metallic Pd in Pd/C-CP was the highest for all the catalysts due to the combined thermal reduction and plasma reduction for catalyst treatment. All of these effects facilitate the diffusion and reaction of formic acid molecules on the Pd active sites to enhance the activity for formic acid dehydrogenation. Therefore, the Pd/C-CP catalyst exhibits the highest activity for formic acid dehydrogenation among the Pd/C catalysts.

For the Pd/C-P catalyst, since the catalyst was treated using plasma reduction only, the negatively-charged $PdCl_4^{2-}$ ions and the formed Pd species could migrate to the outer surface of the AC support despite the strong interaction between the AC and the $PdCl_4^{2-}$ ions. A higher Pd/C atomic ratio was, therefore, obtained for Pd/C-P compared to Pd/C-C (Fig. 3 and Table 2). Pd NPs with a small size and high dispersion can be obtained due to the Coulomb repulsion in the plasma. However, some of the $PdCl_4^{2-}$ ions were not reduced to their active metallic and oxidized states due to the strong interaction between the activated carbon support and the $PdCl_4^{2-}$ ions during plasma treatment. These factors result in poor formic acid dehydrogenation over the Pd/C-P catalyst.

During the preparation of the Pd/C-P catalyst, the interaction between the AC support and the $PdCl_4^{2-}$ ions was destroyed, to some extent, by the migration of the Pd species. Consequently, thermally treating the Pd/C-P catalyst to synthesize Pd/C-PC could result in the aggregation of Pd^0. The mean Pd particle size measured for Pd/C-PC (3.7 ± 1.2 nm) is higher than the reported optimal size of Pd NPs (1.8–3.5 nm),[52] which may explain the poor performance of this catalyst in formic acid dehydrogenation. In conclusion, treating the Pd/C-As precursor by thermal treatment followed by plasma treatment has been demonstrated as an efficient

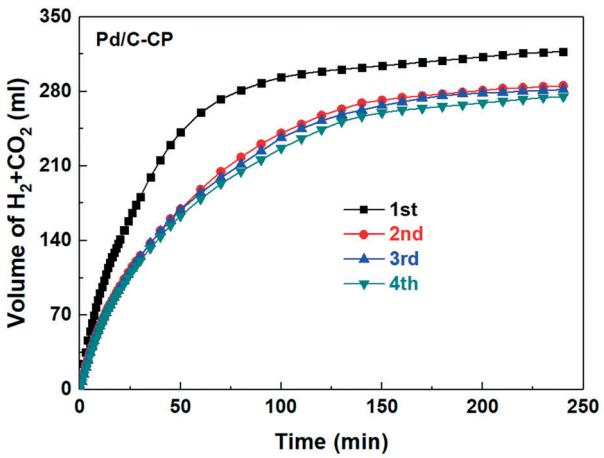

Fig. 9 Stability test (4 reuse cycles) of the Pd/C-CP catalyst at 50 °C.

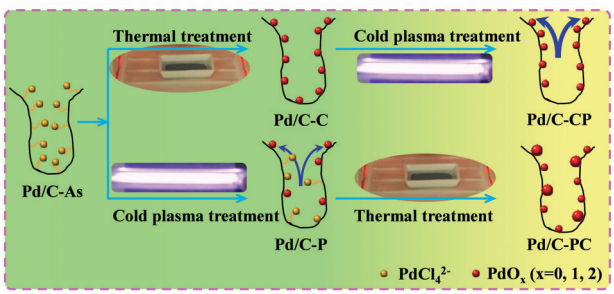

Fig. 10 Schematic illustration of the proposed mechanism for the formation of Pd nanoparticles with different sizes and distributions in the Pd/C catalysts synthesized by different methods.

method for the synthesis of high-performance Pd/C catalysts for the dehydrogenation of formic acid to hydrogen.

Conclusions

Various AC supported Pd catalysts, Pd/C-C, Pd/C-P, Pd/C-CP, and Pd/C-PC, were synthesized by thermal treatment, cold plasma treatment, thermal treatment followed by cold plasma treatment, and cold plasma treatment followed by thermal treatment, respectively. The effect of cold plasma treatment on the Pd/C catalysts has been discussed based on various characterization techniques. The formic acid dehydrogenation activity of the Pd/C catalysts follows the order: Pd/C-CP > Pd/C-C > Pd/C-P > Pd/C-PC. The $TOF_{initial}$ over Pd/C-CP is 1.4, 2.9, and 1.4 times that over Pd/C-C, Pd/C-P and Pd/C-PC, respectively. The significant difference in the catalytic performance is attributed to the strong interaction between the AC support and the $PdCl_4^{2-}$ ions, and the Coulomb repulsion effect of electrons in the plasma. The excellent performance of the Pd/C-CP catalyst is ascribed to the small size and high dispersion of Pd nanoparticles, high concentration of metallic Pd, and the high Pd/C atomic ratio resulting from the migration of the electroneutral Pd species under the Coulomb repulsion effect of electrons in the plasma. In conclusion, thermally treating a Pd/C precursor – obtained using a simple incipient wetness impregnation procedure – followed by plasma treatment is an efficient method for the synthesis of high-performance Pd/C catalysts for the dehydrogenation of formic acid. The apparent activation energy for Pd/C-CP (34.6 ± 1.8 kJ mol^{-1}) is much lower than that reported for other monometallic Pd catalysts. This work provides a promising method for the synthesis of a Pd/C catalyst with a high performance in the dehydrogenation of formic acid, and has great potential to open a green route for controllable synthesis of a range of highly active supported metal catalysts.

Conflicts of interest

There are no conflicts to declare.

Acknowledgements

Support from the National Natural Science Foundation of China (Grant No. 21773020, 21673026, and 11505019), the Liaoning Innovative Talents in University (Grant No. LR2017025), the Natural Science Foundation of Liaoning Province (Grant No. 20180550085) and the UK EPSRC Impact Acceleration Account is greatly appreciated.

Notes and references

1 Global Energy & CO_2 Status Report.
2 C. Liu, Y. Yang, W. Li, J. Li, Y. Li and Q. Chen, *Chem. Eng. J.*, 2016, **302**, 717–724.
3 A. Boddien, B. Loges, F. Gärtner, C. Torborg, K. Fumino, H. Junge, R. Ludwig and M. Beller, *J. Am. Chem. Soc.*, 2010, **132**, 8924–8934.
4 M. Yadav and Q. Xu, *Energy Environ. Sci.*, 2012, **5**, 9698–9725.
5 Z. Li and Q. Xu, *Acc. Chem. Res.*, 2017, **50**, 1449–1458.
6 Y. Yang, H. Xu, D. Cao, X. C. Zeng and D. Cheng, *ACS Catal.*, 2019, **9**, 781–790.
7 M. Guo, Q. Liu, M. Wu, T. Lv and L. Jia, *Chem. Eng. J.*, 2018, **334**, 1886–1896.
8 L. Jia, D. A. Bulushev, S. Beloshapkin and J. R. H. Ross, *Appl. Catal., B*, 2014, **160–161**, 35–43.
9 Y. Chen, Q. L. Zhu, N. Tsumori and Q. Xu, *J. Am. Chem. Soc.*, 2015, **137**, 106–109.
10 D. Gao, Z. Wang, C. Wang, L. Wang, Y. Chi, M. Wang, J. Zhang, C. Wu, Y. Gu, H. Wang and Z. Zhao, *Chem. Eng. J.*, 2019, **361**, 953–959.
11 J. M. Yan, S. J. Li, S. S. Yi, B. R. Wulan, W. T. Zheng and Q. Jiang, *Adv. Mater.*, 2018, **30**, 2–9.
12 B. S. Choi, J. Song, M. Song, B. S. Goo, Y. W. Lee, Y. Kim, H. Yang and S. W. Han, *ACS Catal.*, 2019, **9**, 819–826.
13 A. Bulut, M. Yurderi, Y. Karatas, Z. Say, H. Kivrak, M. Kaya, M. Gulcan, E. Ozensoy and M. Zahmakiran, *ACS Catal.*, 2015, **5**, 6099–6110.
14 L. Xiao, Y. S. Jun, B. Wu, D. Liu, T. T. Chuong, J. Fan and G. D. Stucky, *J. Mater. Chem. A*, 2017, **5**, 6382–6387.
15 Q. Wang, N. Tsumori, M. Kitta and Q. Xu, *ACS Catal.*, 2018, **8**, 12041–12045.
16 Y. Kim and D. H. Kim, *Appl. Catal., B*, 2019, **244**, 684–693.
17 Q. L. Zhu, N. Tsumori and Q. Xu, *Chem. Sci.*, 2014, **5**, 195–199.
18 Y. Wang, M. Craven, X. Yu, J. Ding, P. Bryant, J. Huang and X. Tu, *ACS Catal.*, 2019, **9**, 10780–10793.
19 L. Di, J. Zhang and X. Zhang, *Plasma Processes Polym.*, 2018, **15**, 1700234.
20 Z. Wang, Y. Zhang, E. C. Neyts, X. Cao, X. Zhang, B. W. L. Jang and C. J. Liu, *ACS Catal.*, 2018, **8**, 2093–2110.
21 W. Wang, Z. Wang, J. Wang, C. J. Zhong and C. J. Liu, *Adv. Sci.*, 2017, **4**, 1–9.
22 Y. X. Zeng, L. Wang, C. F. Wu, J. Q. Wang, B. X. Shen and X. Tu, *Appl. Catal., B*, 2018, **224**, 469–478.
23 J. Lian, X. Fang, W. Liu, Q. Huang, Q. Sun, H. Wang, X. Wang and W. Zhou, *Top. Catal.*, 2017, **60**, 831–842.
24 L. Di, Z. Xu, K. Wang and X. Zhang, *Catal. Today*, 2013, **211**, 109–113.
25 Z. Xu, B. Qi, L. Di and X. Zhang, *J. Energy Chem.*, 2014, **23**, 679–683.
26 J. J. Zou, Y. P. Zhang and C. J. Liu, *Langmuir*, 2006, **22**, 11388–11394.
27 L. B. Di, D. Z. Duan, D. W. Park, W. S. Ahn, B. J. Lee and X. L. Zhang, *Top. Catal.*, 2017, **60**, 925–933.
28 S. Zhang, X. S. Li, B. Zhu, J. L. Liu, X. Zhu, A. M. Zhu and B. W. L. Jang, *Catal. Today*, 2015, **256**, 142–147.
29 V. D. Dao, C. Q. Tran, S. H. Ko and H. S. Choi, *J. Mater. Chem. A*, 2013, **1**, 4436–4443.
30 W. Wang, Z. Wang, M. Yang, C. J. Zhong and C. J. Liu, *Nano Energy*, 2016, **25**, 26–33.
31 Y. X. Pan, H. P. Cong, Y. L. Men, S. Xin, Z. Q. Sun, C. J. Liu and S. H. Yu, *ACS Nano*, 2015, **9**, 11258–11265.

32 L. Di, X. Zhang, B. Lee, P. Lu, W. S. Ahn and D. W. Park, *Plasma Chem. Plasma Process.*, 2017, **37**, 1535–1549.
33 L. Di, Z. Li, B. Lee and D. W. Park, *Int. J. Hydrogen Energy*, 2017, **42**, 11372–11378.
34 W. Chu, L. N. Wang, P. A. Chernavskii and A. Y. Khodakov, *Angew. Chem., Int. Ed.*, 2008, **47**, 5052–5055.
35 J. Hong, W. Chu, P. A. Chernavskii and A. Y. Khodakov, *J. Catal.*, 2010, **273**, 9–17.
36 J. Hong, J. Du, B. Wang, Y. Zhang, C. Liu, H. Xiong, F. Sun, S. Chen and J. Li, *ACS Catal.*, 2018, **8**, 6177–6185.
37 X. Fang, J. Lian, K. Nie, X. Zhang, Y. Dai, X. Xu, X. Wang, W. Liu, C. Li and W. Zhou, *J. Energy Chem.*, 2016, **25**, 825–831.
38 Y. Xu, Y. Chen, J. Li, J. Zhou, M. Song, X. Zhang and Y. Yin, *Int. J. Hydrogen Energy*, 2017, **42**, 13085–13091.
39 W. Chu, J. Xu, J. Hong, T. Lin and A. Khodakov, *Catal. Today*, 2015, **256**, 41–48.
40 L. Di, Z. Xu and X. Zhang, *Catal. Today*, 2013, **211**, 143–146.
41 B. Qi, L. Di, W. Xu and X. Zhang, *J. Mater. Chem. A*, 2014, **2**, 11885–11890.
42 W. Xu, Z. Zhan, L. Di and X. Zhang, *Catal. Today*, 2015, **256**, 148–152.
43 L. Di, X. Zhang, Z. Xu and K. Wang, *Plasma Chem. Plasma Process.*, 2014, **34**, 301–311.
44 L. Di, D. Duan, X. Zhang, B. Qi and Z. Zhan, *IEEE Trans. Plasma Sci.*, 2016, **44**, 2692–2698.
45 L. Di, J. Zhang, C. Ma, X. Tu and X. Zhang, *Catal. Today*, 2019, **337**, 201–207.
46 B. S. Ahn, S. G. Jeon, H. Lee, K. Y. Park and Y. G. Shul, *Appl. Catal., A*, 2000, **193**, 87–93.
47 M. I. Cobo, J. A. Conesa and C. M. De Correa, *J. Phys. Chem. A*, 2008, **112**, 8715–8722.
48 L. Wang, Y. Yi, H. Guo and X. Tu, *ACS Catal.*, 2018, **8**, 90–100.
49 X. Wang, G. W. Qi, C. H. Tan, Y. P. Li, J. Guo, X. J. Pang and S. Y. Zhang, *Int. J. Hydrogen Energy*, 2014, **39**, 837–843.
50 J. Gu, S. Wang, Z. He, Y. Han and J. Zhang, *Catal. Sci. Technol.*, 2016, **6**, 809–817.
51 C. Hu, J. K. Pulleri, S. W. Ting and K. Y. Chan, *Int. J. Hydrogen Energy*, 2014, **39**, 381–390.
52 F. Sanchez, D. Motta, A. Roldan, C. Hammond, A. Villa and N. Dimitratos, *Top. Catal.*, 2018, **61**, 254–266.
53 Q. L. Zhu, N. Tsumori and Q. Xu, *J. Am. Chem. Soc.*, 2015, **137**, 11743–11748.